Aromatic Ring Cleavage by Homoprotocatechuate 2,3-Dioxygenase: Role of His200 in the Kinetics of Interconversion of Reaction Cycle Intermediates†

Stephanie L. Groce‡ and John D. Lipscomb*

Department of Biochemistry, Molecular Biology, and Biophysics, and Center for Metals in Biocatalysis, University of Minnesota, Minneapolis, Minnesota 55455

Received January 29, 2005; Revised Manuscript Received March 21, 2005

ABSTRACT: Homoprotocatechuate 2,3-dioxygenase (WT 2,3-HPCD) isolated from *Brevibacterium fuscum* utilizes an active site Fe(II) and O_2 to catalyze proximal extradiol cleavage of the aromatic ring of the substrate (HPCA). Here, the conserved active site residue His200 is changed to Gln, Glu, Ala, Asn, and Phe, and the reactions of the mutant enzymes are probed using steady-state and transient kinetic techniques. Each mutant catalyzes ring cleavage of HPCA to yield the normal product. H200Q and H200N retain 30−40% of the WT 2,3-HPCD activity at 24 °C, but the other mutants reduce the k_{cat} to less than 9% of normal. The origin of the reduced activity is unlikely to be the substrate binding phase of the catalytic cycle, because the multistep anaerobic binding reaction of the chromophoric substrate 4-nitrocatechol (4NC) is shown to proceed with rate constants similar to those observed for WT 2,3-HPCD. In contrast, the rate constants of several steps in the multistep O_2 binding/insertion and product release half of the reaction cycle are substantially slowed, in particular the steps in which activated oxygen attacks the organic substrate and in which product is released. In the case of the H200N mutant, the product of 4NC oxidation is not the usual ring cleavage product, but rather the 4NC quinone. These results suggest that the main role of His200 is in facilitating the steps in the second half of the reaction cycle. The decreased rate constants for the O_2 insertion steps in the catalytic cycles of the mutant enzymes allow the oxygen adduct of an extradiol dioxygenase to be detected for the first time.

Homoprotocatechuate 2,3-dioxygenase (2,3-HPCD[1]) isolated from *Brevibacterium fuscum* is an Fe(II) containing extradiol dioxygenase that catalyzes the O_2-dependent ring opening of its aromatic substrate (HPCA) as shown (*1*):

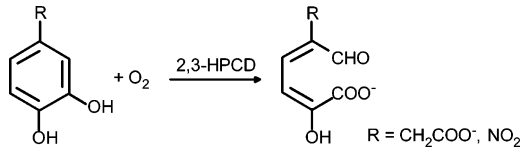

The enzyme is a member of the type I extradiol dioxygenase class (*2*) which includes catechol 2,3-dioxygenase, the dihydroxybiphenyl 1,2-dioxygenases from *Pseudomonas* sp. KKS102 (BphC) and *Burkholderia* sp. LB400 (DHBD), and homoprotocatechuate 2,3-dioxygenase from *Arthrobacter globiformis* (MndD), an enzyme with high sequence homology to 2,3-HPCD but with Mn(II) rather than Fe(II) in the active site (*3*). Each of these enzymes has been structurally characterized (*4*−*8*) and shown to bind the active site metal in a 2-His-1-carboxylate facial triad motif common to many mononuclear metalloenzymes (*9*). Spectroscopic and structural studies of the substrate complexes showed that the vicinal hydroxyl groups bind to the iron in a highly asymmetric chelate complex, suggesting that only one group ionizes (*7*, *8*, *10*, *11*). We have proposed that this occurs because the starting neutral charge of the metal center is maintained if only one of the two hydroxyl groups of the substrate becomes ionized during the binding process (*12*, *13*). As substrates bind, it appears that two or three solvent molecules are released from the metal coordination (*8*). This results in a 5-coordinate metal center with a vacant site next to the substrate ligand sites that is presumably used to bind and activate O_2. This hypothesis has been strongly supported by structural studies of the ternary substrate−nitrosyl complex of BphC which shows NO binding immediately adjacent to the bond that would be cleaved in the normal reaction (*7*).

† This work was supported by National Institutes of Health Grant GM24689 (J.D.L.). S.L.G. was supported in part by NIH Training Grant GM008347.

* To whom correspondence should be addressed. Mailing address: University of Minnesota, Department of Biochemistry, Molecular Biology, and Biophysics, 6-155 Jackson Hall, 321 Church St. SE, Minneapolis, MN 55455. E-mail: lipsc001@umn.edu. Tel: (612) 625-6454. Fax: (612) 624-5121.

‡ Current address: Cancer Center, University of Minnesota, Minneapolis, MN 55455.

[1] Abbreviations: 4NC, 4-nitrocatechol; HPCA, homoprotocatechuate or 3,4-dihydroxyphenylacetate; PCA, protocatechuate; MOPS, 3-morpholinopropanesulfonic acid; 2,3-HPCD, homoprotocatechuate 2,3-dioxygenase from *Brevibacterium fuscum*; MndD, homoprotocatechuate 2,3-dioxygenase from *Arthrobacter globiformis*; DHBD, dihydroxybiphenyl 1,2-dioxygenase from *Burkholderia* sp. LB400; BphC, dihydroxybiphenyl 1,2-dioxygenase from *Pseudomonas* sp. KKS102; E, E′, E−4NC(1), E′−4NC(1), E−4NC(2), and E−4NC(3), enzyme intermediates formed during 4NC binding to 2,3-HPCD; E−4NC−O_2(1), E−4NC−O_2(2), E−4NC−O_2(3), enzyme intermediates formed during the oxygen binding and product forming segment of the 2,3-HPCD turnover reaction with 4NC; the same abbreviations with HPCA substituted for 4NC apply to the reaction with the native substrate; RRT, reciprocal relaxation time.

10.1021/bi050180v CCC: $30.25
Published on Web 04/20/2005

Scheme 1: Proposal for the Reaction Cycle of Extradiol Ring Cleaving Dioxygenases

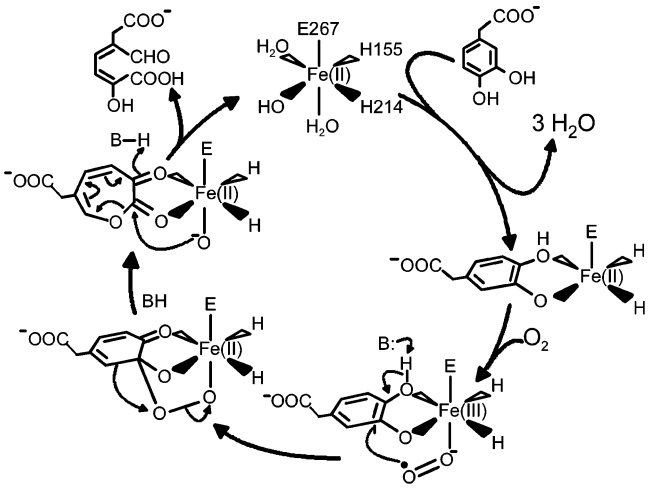

Chart 1: Active Site Region of *B. fuscum* 2,3-HPCD Showing the Substrate Binding Position Relative to the Fe(II) and the Conserved Second Sphere His200[a]

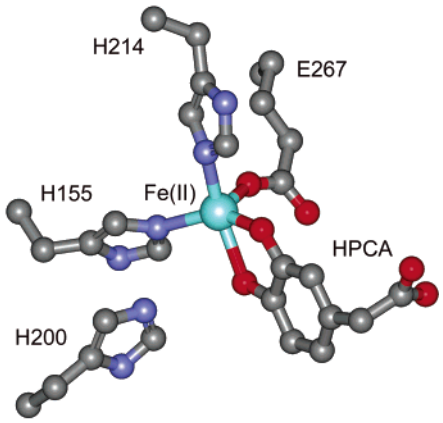

[a] Structures from ref *8*. PDB entry 1Q0C.

The mechanism of extradiol ring cleaving dioxygenases remains unknown, although many advances have been made in recent years. As shown in Scheme 1, we have proposed that electron density is transferred from the substrate to the bound O_2 through the metal to which they are both bound (*10*, *14*, *15*). Subsequent nucleophilic attack of the nascent superoxide on the slightly electron deficient substrate at the eventual site of ring opening would lead to an alkyl−peroxy intermediate. This intermediate would undergo heterolytic O−O bond cleavage with insertion of one oxygen atom into the ring to form a lactone intermediate via a Criegee rearrangement reaction (*16*). Such a reaction would be facilitated if the second substrate hydroxyl ionized, thereby transferring additional electron density into the ring. Finally, hydrolysis of the lactone intermediate by the second atom of oxygen, which is retained on the metal at the level of water, would yield the ring-open semialdehyde product. Several experimental observations support this overall scheme including greatly increased affinity for NO upon substrate binding (*17*), partial exchange of ^{18}O from labeled O_2 consistent with a two-step oxygen insertion process, and evidence for radical character on the aromatic ring prior to ring cleavage (*18*, *19*).

While this type of mechanism could be carried out exclusively by the metal with bound substrate and O_2, second sphere amino acid side chains might play several types of roles in catalysis (*4*, *7*, *20*, *21*). Four general types of roles would be (i) to serve as an active site base to promote formation of the monoanionic substrate complex and/or remove the hydroxyl proton suggested above to facilitate the Criegee rearrangement chemistry, (ii) to stabilize the oxygen complex by hydrogen bonding, (iii) to serve as an active site acid to promote the heterolytic O−O bond breaking reaction of the metal-bound oxygen atom, and (iv) to orient the substrates through steric interactions to promote oxygen attack and to determine the site of ring opening.

The X-ray crystal structure of the BphC−substrate complex showed that the highly conserved His194 was well-positioned to participate in several of these possible roles, and it was suggested that it might remove the proton from the second hydroxyl group of the substrate and donate this proton to the oxygen during O−O bond cleavage (*7*). Others also noted the proximity of His194 or its equivalent to vacant iron site in the substrate complex (*4*, *21*−*23*) as shown for 2,3-HPCD in Chart 1.

In a previous study, we showed that mutation of the equivalent histidine (His200) in 2,3-HPCD to Phe (H200F) promoted a change from extradiol to intradiol ring cleavage for the alternative substrate 2,3-dihydroxybenzoate, while preserving the extradiol cleavage of HPCA (*20*). The latter studies showed that a residue capable of acid−base chemistry is not required at position 200 to allow substrate binding and ring opening. Nevertheless, the reaction was substantially slowed in the mutant enzyme. The fact that the position of ring opening was altered in some cases supported a structural role for the residue at this position. Finally, it was noted that the Fe(II) rapidly oxidized during turnover of the H200F mutant, suggesting that the His200 residue might play a role in either stabilizing the oxygen complex or accelerating its reaction with substrate, thereby preventing adventitious loss of superoxide.

Recently, we have studied the extradiol mechanism of 2,3-HPCD by using the chromophoric alternative substrate 4-nitrocatechol (4NC) (*12*). The relatively intense chromophore of 4NC changes dramatically as the hydroxyl groups ionize (*24*) and exhibits more subtle changes due to alterations in the environment of the ionized forms. Moreover, the product of the ring opening reaction exhibits another unique spectrum. Consequently, the complex substrate binding process and the subsequent oxygen binding, ring opening, and product release steps could be followed in detail using single turnover transient kinetic techniques. The substrate binding process was shown to consist of at least 4 steps including a conversion of the monoanionic form of 4NC found in solution at neutral pH to a bound dianionic form. This difference in the bound ionization state of 4NC versus HPCA is likely to be principally due to the difference in pK_a values for the hydroxyl functions of the two substrates, but it may also reflect the characteristics of the base(s) present in the active site to facilitate the deprotonation reaction. The oxygen reaction phase of the reaction cycle was also found to consist of at least 4 steps. The number and spectral characteristics of the intermediates observed in the reaction cycle are consistent with the mechanistic proposal of Scheme 1. Unfortunately, the initial substrate and O_2 binding steps were not directly detected, and their

Table 1: Oligonucleotides Used To Construct Site-Directed Mutations in 2,3-HPCD

mutation[a]	oligonucleotide primer[b]
H200A+	5′CGTTGCCGCCGGTCAGGGCGGTGTC**GGT**CACGGTGCCCTTGC3′
H200A−	5′CCTGGATGCACCGCAAGGGCACCGTG**GCC**GACACCGCCCTG3′
H200N+	5′CGGTCAGGGCGGTGTC**GTT**CACGGTGC3′
H200N−	5′CCGCAAGGGCACCGTG**AAC**GACACCGCCC3′
H200Q+	5′CGGTCAGGGCGGTGTC**CTG**CACGGTGC3′
H200Q−	5′CCGCAAGGGCACCGTG**CAG**GACACCGCCC3′
H200E+	5′CGTTGCCGCCGGTCAGGGCGGTGTC**CTC**CACGGTGCCCTTGC3′
H200E−	5′CCTGGATGCACCGCAAGGGCACCGTG**GAG**GACACCGCCCTG3′
H200F+	5′CGTTGCCGCCGGTCAGGGCGGTGTC**GAA**CACGGTGCCCTTGC3′
H200F−	5′CCTGGATGCACCGCAAGGGCACCGTG**TTC**GACACCGCCCTG3′

[a] All mutants were constructed in plasmid pYZW204. [b] Mutant codons are in bold letters.

presence and rate constants were inferred on the basis of analysis of the kinetics of the following step. Consequently, the critical initial ES and ES−O_2 intermediates could not be characterized.

In the study presented here, the role of the position 200 residue in 2,3-HPCD is probed using a variety of mutations at this position. By monitoring the transient kinetics of single turnover of 4NC and HPCA, the specific steps in the turnover cycle most affected by the chemical nature of the position 200 side chain are directly determined. Significantly, for specific mutants, the O_2 binding and/or reaction steps are slowed such that they can be directly observed for the first time. Finally, it is shown that this is also true when the native substrate HPCA is used, allowing the key reactive oxygen adduct of the 2,3-HPCD reaction cycle to be detected for the first time.

EXPERIMENTAL PROCEDURES

Reagents. All chemicals were purchased from Sigma-Aldrich and were used without purification except for HPCA, PCA, and 4NC, which were recrystallized from water at 4 °C to remove minor contaminants. Protocatechuate 3,4-dioxygenase was purified as previously described (*25*). Anaerobic conditions were achieved by repeated cycling of solutions between argon gas and vacuum. Trace contaminating O_2 was removed from the Ar gas by passage over a BASF copper catalyst at 150 °C.

Site-Directed Mutagenesis. The primers used to create the 2,3-HPCD His200 mutants are listed in Table 1 and were synthesized in the Microchemical Facility at the University of Minnesota. All mutations were created in the plasmid pYZW204 (*26*) using the QuikChange Site-Directed Mutagenesis Kit (Stratagene). The desired mutation was verified by gene sequence analysis performed in the Microchemical Facility at the University of Minnesota. The sequencing primer designed for verification of desired His200 mutations is 5′CGTACGAGTTCTTCTTCGAGACC3′.

Overexpression of WT 2,3-HPCD and His200 Mutants in Escherichia coli and Purification. WT 2,3-HPCD and His200 mutants were overexpressed in *E. coli* strain BL21 (DE3) and subsequently purified as previously described for the wild-type enzyme (*26*).

Enzyme and Metal Quantification. The concentration of purified WT 2,3-HPCD and His200 mutants was routinely determined using the absorbance at 280 nm ($\epsilon = 1.14$ mg^{-1} ml cm^{-1}). The optical absorption was measured using a Hewlett-Packard 8453 spectrophotometer. Metal was quantified using a Varian SpectrAA-100 flame atomic absorption spectrometer at 248.3 nm.

Steady-State Kinetic Measurements. Wild-type and mutant enzymes were assayed for dioxygenase activity as previously described (*12*). Briefly, either the rate of O_2 consumption was monitored by using a Clark-type oxygen electrode (*25*) or the rate of product formation was directly monitored at 380 nm ($\epsilon_{380} = 36\,000$ M^{-1} cm^{-1}, pH 7.5). 4NC turnover activity was measured at pH 7.5 at 330 nm using $\Delta\epsilon_{330} = 12\,060$ M^{-1} cm^{-1}, which is the difference extinction coefficient for 4NC (1840 M^{-1} cm^{-1}) and product (13 900 M^{-1} cm^{-1}). Standard assay conditions were 22 °C, 50 mM MOPS, pH 7.5 although determinations were also made at 4 °C for comparison with the transient kinetic results. Initial velocity data were analyzed as a hyperbolic function of substrate concentration to determine K_m and V_{max} using KFIT, a nonlinear regression program developed by Neil C. Millar (King's College, London, U.K.).

Determination of the Dissociation Constant for 4NC. The K_d for 4NC binding to the mutant forms of 2,3-HPCD was determined by monitoring changes in the 4NC optical spectrum as previously described (*12*).

Transient Kinetic Experiments. All experiments, except where noted, were conducted under pseudo first order conditions using an Applied Photophysics model SX.18MV stopped-flow device at 4 °C. The reaction conditions and analysis procedures were as previously described (*12*). Reciprocal relaxation times (RRTs) and amplitudes were determined by simulating time courses summed exponential functions using nonlinear regression. The total number of exponential terms and RRT values ($1/\tau_n$) is equal to the number of steps in the actual reaction as long as no internal cycles occur. The order of the exponential phases is not necessarily the order of the steps in the reaction.

For pH-dependent turnover and transient kinetic studies, measurements were carried out over the pH range of 5.5 to 10.0. All buffers were prepared at a concentration of 50 mM, and the conductivity of all buffers was adjusted to a constant value with a minimal amount of 3 M NaCl. The measured conductivity of the buffers was 645 ± 12.3 μS/cm. Buffers used were MES (pH 5.5 to 6.3), MOPS (pH 6.6 to 7.5), TAPS (pH 7.8 to 8.7), and CHES (pH 9.0 to 10.0).

RESULTS AND ANALYSIS

Residue His200 was replaced with Ala, Gln, Asn, Glu, and Phe by site-directed mutagenesis, and each mutant enzyme was overexpressed in high yield and purified to

Table 2: Kinetic Parameters of Turnover of HPCA by WT 2,3-HPCD and Its H200 Mutants at Room Temperature[a]

parameter	wild-type	H200A	H200Q	H200N	H200E	H200F
k_{cat} (s^{-1})	10 ± 1	0.3 ± 0.04	4 ± 0.3	3 ± 0.3	0.9 ± 0.1	0.21 ± 0.03
K_{mHPCA} (μM)	30 ± 2	5 ± 0.5	28 ± 2	10 ± 1	0.4 ± 0.05	31 ± 2
pK_{a1}	7.1 ± 0.1	6.5 ± 0.1	7.0 ± 0.1	7.0 ± 0.1	7.0 ± 0.1	6.5 ± 0.1
K_{d4NC} (μM)[b]	5 ± 2	10 ± 2.7	14 ± 2	2 ± 0.5	10 ± 3	11 ± 2

[a] The kinetic parameters (k_{cat} and K_m) were determined spectrophotometrically by following product formation at 380 nm. Reactions were carried out in 50 mM MOPS, pH 7.5 and the reaction was monitored at 24 °C. The initial velocity measurements as a function of pH were determine polarographically under steady-state conditions at 24 °C. V_{max} values determined from the data were converted to k_{cat} values using the concentration of Fe(II) to indicate the functional active site concentration. [b] The dissociation constants for 4NC binding were determined as described in Experimental Procedures.

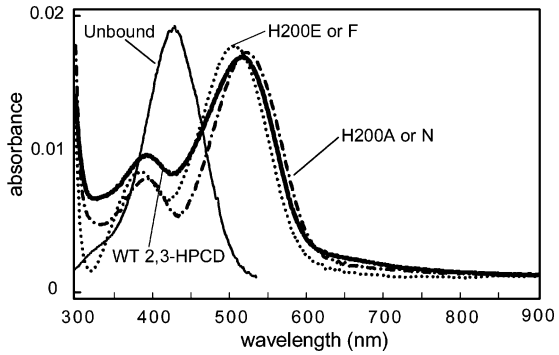

FIGURE 1: Optical spectra of anaerobic H200X−4NC complexes at pH 7.5. The spectra of WT 2,3-HPCD−4NC and unbound 4NC are shown for comparison. Enzyme and 4NC are 30 μM (Fe(II) sites) and 5 μM, respectively, in 50 mM MOPS, pH 7.5, 24 °C.

apparent homogeneity as described in Experimental Procedures. Only a single band was observed for each mutant after silver stained SDS−PAGE, and circular dichroism spectra revealed no changes in the secondary structure content with respect to WT 2,3-HPCD (data not shown).

Steady-State Kinetics of HPCA Turnover. Each of the H200 mutants retains extradiol dioxygenase activity to yield the same product as observed for WT 2,3-HPCD when HPCA is used as the substrate. Table 2 lists the steady-state kinetic parameters determined for these mutant enzymes and WT 2,3-HPCD. H200Q and H200N retain a significant amount of activity with k_{cat} values being approximately 40% and 30% of that of WT 2,3-HPCD, respectively. H200A, H200E, and H200F show much lower activity, retaining only 3%, 9%, and 2.1% activity, respectively at pH 7.5. The p*K*a values for the changes in k_{cat} with pH for HPCA turnover are also listed in Table 2. The K_{mHPCA} values for the H200 mutants are either similar to or lower than those for WT 2,3-HPCD, suggesting that this residue does not significantly affect formation of the Michaelis complex.

Anaerobic H200X−4NC Complexes. We recently reported that the chromophoric substrate 4-nitrocatechol (4NC) binds to WT 2,3-HPCD at pH 7.5 as a dianion despite the fact that the natural substrate, HPCA, binds as a monoanion (*12*). As shown in Figure 1, each mutant also binds 4NC as a dianion with only minor changes in the optical spectra compared to that of the WT 2,3-HPCD−4NC complex. The apparent K_d values for 4NC binding to H200 mutants determined by monitoring the shift from monoanion (predominant state in solution) to dianion as 4NC binds (see ref *12*) are listed in Table 2. The mutations cause only small changes in the affinity for this alternative substrate. Thus, it appears that the mutation of the residue at position 200 has little effect on either the protonation state of the bound 4NC or its affinity. The high affinity exhibited for 4NC facilitates the transient kinetic experiments described below.

Reaction Cycle Transient Kinetics. On the basis of the steady-state kinetics of extradiol dioxygenase systems, the binding process is believed to be ordered with the catecholic substrate binding first (*27*). Consequently, the single turnover reaction of 4NC is conveniently monitored as two half-reactions: anaerobic substrate binding and reaction of the preformed enzyme substrate complex with O_2. The kinetic data for these two half-reactions will be presented and analyzed in the following sections, and then put into the context of mechanism in the Discussion.

Transient Kinetics of Complex Formation. The time course of the first half-reaction was monitored at 4 °C, pH 7.5 under pseudo first order conditions with 4NC in large excess; a typical time course is shown for the H200N reaction in Figure 2. When monitored over a 0.5 s interval (Figure 2A), the time course is best fit by three summed exponentials. The plot of the fastest RRT versus 4NC concentration shown in Figure 3A is linear, suggesting that the step in which 4NC binds to the enzyme has rate constants given by the slope and intercept of the plot ($k_{binding} = 80\,000 \pm 6000\ M^{-1}\ s^{-1}$, $k_{release} = 46 \pm 6\ s^{-1}$).

When the reaction was monitored over a 10 s interval as shown in Figure 2B, the data were again best fit by a summed three exponential function. However, the fastest and next fastest RRTs correlate with the second and third fastest phases of the data recorded over the shorter interval. Presumably, there are too few points at short times to resolve the initial binding phase in the data recorded on a 10 s time scale. Taken together, the data reveal four exponential phases, meaning that there must be at least four steps in the binding reaction. We have shown previously that this is also true for the 4NC binding to WT 2,3-HPCD, although in that case the fastest phase was implied by the data and not directly detected (*12*). The binding of 4NC to WT 2,3-HPCD was reexamined during the current study under the conditions used for the mutant enzymes. The fast phase with a linear concentration dependence on 4NC was detected with the rate constants $k_{binding} = 58\,000 \pm 7000\ M^{-1}\ s^{-1}$, $k_{release} = 10 \pm 5\ s^{-1}$. The RRTs observed for the slowest three phases of the reactions reported here for the mutant enzymes are similar to those observed for 4NC binding to WT 2,3-HPCD, as shown in Table 3.

Plots of the RRTs for the three slowest phases as a function of 4NC concentration for the reaction using the mutant H200N are shown in Figure 3B−D. As observed for WT 2,3-HPCD, the fastest of these three phases for the H200N reaction shows a hyperbolic dependence on 4NC concentration while the second fastest shows no concentration

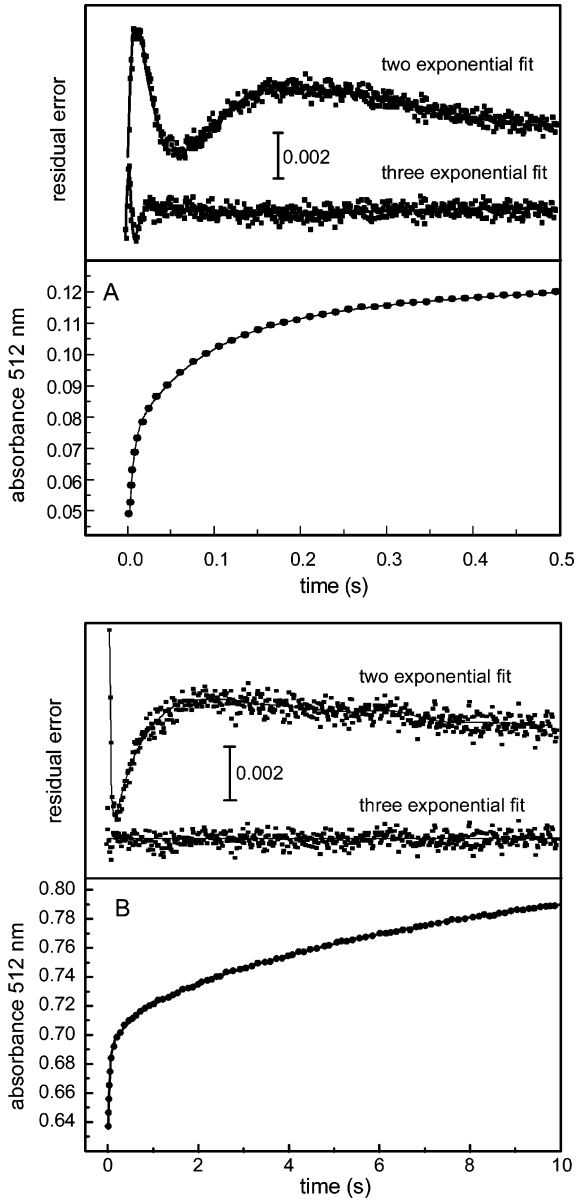

FIGURE 2: Single wavelength trace of the binding reaction of 4NC to H200N under pseudo first order conditions over (A) 0.5 s and (B) 10 s intervals. 4NC and H200N (Fe(II) sites) were present at 3.2 mM and 20 μM, respectively, after rapid mixing using a stopped flow device. Samples were prepared in 50 mM MOPS, pH 7.5, and the reaction was monitored at 4 °C. The trace was fit to two and three- exponential equations, and the residuals are shown for each time interval. Approximately every 5th point (dots) is shown for the data sets.

dependence. Interestingly, the slowest phase appears to exhibit a hyperbolic concentration dependence in the case of H200N, whereas it was found to be concentration independent in the case of the wild-type enzyme (*12*). The hyperbolic dependence of the fastest of these three phases suggests that it derives primarily from the step after the true first step in the binding process. If this is the case, then analysis of the data shown in Figure 3B using eq 1 gives values of $K_d = 500 \pm 100$ μM for the true association step and $k_{forward} = 80 \pm 10$ s^{-1}, $k_{reverse} = 2 \pm 2$ s^{-1} for the second step.

$$1/\tau_{obs} = k_{forward}(4NC)/(K_d + 4NC) + k_{reverse} \qquad (1)$$

The K_d value calculated from the forward and reverse rate constants of the directly observed first binding step is 575 μM, in good agreement with this analysis. However, the fact that the observed overall K_d is much smaller (Table 2) shows that the following steps are important for the overall binding process, and that they are greatly favored in the forward direction. These can be analyzed in more detail by considering the slower observed phases of the binding reaction data.

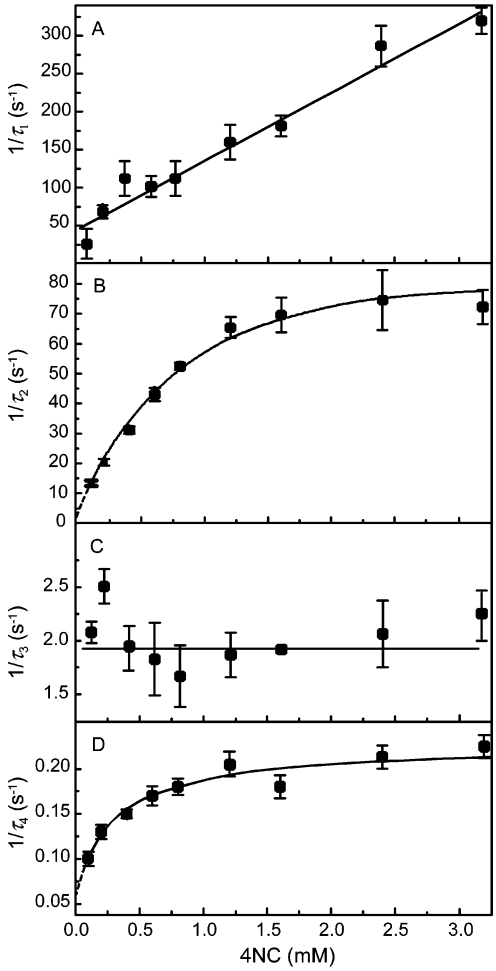

FIGURE 3: Reciprocal relaxation times for the anaerobic formation of H200N−4NC plotted as a function of 4NC concentration. H200N (20 μM sites after mixing) was reacted with 4NC (80 μM to 2.4 mM after mixing). The reactions were carried out in 50 mM MOPS, pH 7.5 and monitored at 4 °C.

In our previous study of 4NC binding to WT 2,3-HPCD, we argued that the process is unexpectedly complex (*12*). On the basis of analysis of the 4NC concentration dependence and the pH dependence of the relative amplitudes of the observed phases, it was proposed that the reaction occurs as shown in Scheme 2.

The E and E′ enzyme forms are proposed to be related by the ionization of an amino acid residue or solvent ligand which is important for binding. In Scheme 2, the absence of the ionized residue in the E′ form greatly slows the formation of the dianionic 4NC complex and ultimately is the major contributor to the slowest exponential phase in the fitting of the binding time course. This scheme predicts that there will be two phases with a nonlinear 4NC concentration dependence, whereas only one was actually observed.

The results presented here show that the 4NC binding reaction for H200N follows a course similar to that of WT 2,3-HPCD. While equally complex, the reaction scheme is more easily evaluated due to the facts that (i) the true

Table 3: Reciprocal Relaxation Times and Amplitudes Derived from Single Wavelength Traces Monitoring the Reaction of Anaerobic E−4NC Formation over a 10 s Time Interval[a]

	wild-type		H200A		H200E		H200F[d]		H200N	
phase[b]	$1/\tau$ (s^{-1})	amp[c] (%)	$1/\tau$ (s^{-1})	amp (%)	$1/\tau$ (s^{-1})	amp (%)	$1/\tau$ (s^{-1})	amp (%)	$1/\tau$ (s^{-1})	amp (%)
2	42 ± 2	44.5	20 ± 3	42.2	31 ± 4	51.8	10 ± 2	42	82 ± 10	21.2
3	1.9 ± 0.1	4.5	2.4 ± 0.2	6.7	1.6 ± 0.5	25.3	3.2 ± 0.5	17.5	1.9 ± 0.3	19.2
4	0.15 ± 0.02	42.2	0.13 ± 0.02	51.1	0.32 ± 0.05	22.9	0.19 ± 0.04	40.5	0.23 ± 0.03	59.6

[a] The reaction was monitored at 512 nm over a 10 s time course. Wild-type and mutants were 20 μM upon mixing with 3.2 mM 4NC (except where noted) under anaerobic conditions. The reaction was monitored at 4 °C, and samples were prepared in 50 mM MOPS, pH 7.5. [b] The reaction contains another phase that is significantly faster than those shown here. [c] Amplitudes are expressed as % of overall change. The amplitude of the fast initial phase[b] is not accounted for in these data. [d] 4NC was at a concentration of 600 μM and not saturating.

Scheme 2: Proposed Steps in the Anaerobic Binding of 4NC to WT 2,3-HPCD (*12*)

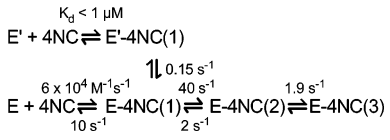

Scheme 3: Proposed Steps and Rate Constants for the Anaerobic Binding of 4NC to H200N

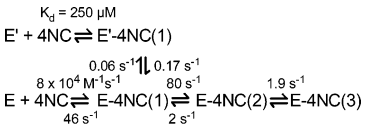

substrate binding step can be directly observed for at least one of the enzyme forms and (ii) there are now two slower phases that exhibit hyperbolic concentration dependence on 4NC (Figure 3B,D). In the case of the H200N mutant, analysis of the hyperbolic plot shown in Figure 3D suggests that the binding reaction of the putative protonated form E′ is reversible with a K_d value of approximately 250 μM, and $k'_{forward}$ and $k'_{reverse}$ values of 0.17 and 0.06 s^{-1}, respectively.

One alternative to Scheme 2 would be a linear series of reactions from binding through formation of the final complex. The near zero reverse rate for the second step in the reaction given by analysis of the data shown in Figure 3B would account for the loss of concentration dependence in the phase shown in Figure 3C. However, two facts suggest that this interpretation is incorrect. First, the irreversible step would result in the loss of concentration dependence in both of the slower phases for a linear series of steps. Second, the spectral changes observed during the reaction indicate that only about half of the conversion of 4NC to the dianion occurs in the second step (see Figure 2). This seems unlikely for a linear series of steps, given that the conversion of the monoanion to the dianion is a single step process.

As in the case of the WT enzyme, the amplitudes of the two concentration dependent phases that follow the first fast binding phase for the H200N mutant reaction exhibit strong but opposite pH dependencies such that the faster process leading to formation of dianionic 4NC dominates at high pH (data not shown). This shows that His200 is not the ionizable residue that affects the distribution of the putative E and E′ enzyme forms.

The rate constants for the 4NC binding reaction to H200N are summarized in Scheme 3. Comparison with those shown in Scheme 2 for WT 2,3-HPCD (also see Table 3) suggests that the substrate binding reactions are very similar with the rate-limiting steps occurring with rate constants differing by less than a factor of 2. This suggests that His200 has relatively small effects on the substrate binding process and, specifically in the case of 4NC, does not perform the potential role described in the introduction of acting as an essential active site base to deprotonate incoming substrate. Accordingly, as shown in Table 3, each of the mutants binds 4NC as a dianion in a series of very similar steps with similar rate constants despite the fact that most residue 200 substitutes are not effective bases in the neutral pH range. The actual base that facilitates this process is not known, but we have hypothesized that the critical ionizing group may be one or more solvents in the coordination sphere of the iron (*12*).

Single Turnover of Preformed H200N−4NC Complex upon Exposure to O_2. The second half of the single turnover reaction was studied by first forming the anaerobic, stoichiometric E−4NC(3) complex in one stopped-flow syringe using a concentration well above the overall K_d for the complex (Table 2). This was then rapidly mixed with O_2-containing buffer from the second syringe under pseudo first order conditions. In this way, only a single turnover was permitted beginning from the final E−4NC(3) complex. A multiphase process was observed. Time segments of diode array traces of the reaction are shown in Figure 4. In the very early time segment of the reaction (Figure 4A), there is a small absorbance increase in the 450 nm region with a concomitant decrease at 520 nm and isosbestic points at 495 and 580 nm, indicating the formation of a transient intermediate. The absorbance maximum shifts from 518 to 506 nm in a process that is almost complete by 24 ms. This is a novel intermediate not observed during the analogous reaction using the WT 2,3-HPCD. Over the next 10 s (Figure 4B), the spectrum undergoes a subtle change with an isosbestic point at 460 nm indicative of another intermediate that absorbs at the same maximum wavelength, but has a smaller extinction coefficient.

A single wavelength trace is shown in Figure 5A for the reaction of E−4NC with 700 μM O_2 recorded at 450 nm over a 1 s interval. The trace was fit by two summed exponentials to yield RRTs of $1/\tau_1 = 160 \pm 20$ s^{-1}, $1/\tau_2 = 0.22 \pm 0.04$ s^{-1}. As shown in Figure 5B, the faster observable phase shows a linear dependence on O_2 concentration, suggesting that the O_2 binding reaction is directly observed. The slope of this plot gives a second-order rate constant for the reaction of $k_{binding} = (1.5 \pm 0.2) \times 10^5$ M^{-1} s^{-1} and the intercept gives a reverse rate constant $k_{release} = (52 \pm 5)$ s^{-1} ($K_d = 340$ μM) (Table 4).

The observation of two phases might indicate that there are two successive steps in this part of the reaction. However,

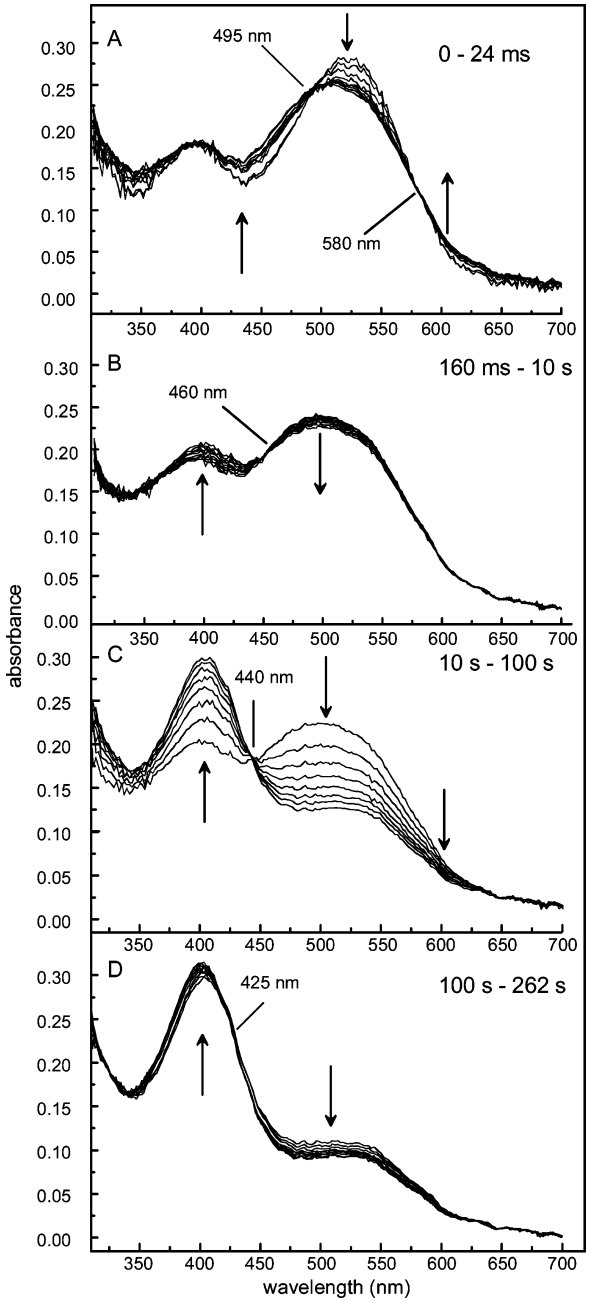

FIGURE 4: Time segments of the rapid scan diode array spectra of the reaction of preformed H200N−4NC with O_2. The preformed complex (30 μM sites after mixing) was mixed with O_2-saturated buffer in 50 mM MOPS, pH 7.5, 4 °C. Arrows indicate direction of absorbance change, and approximate isosbestic points are marked.

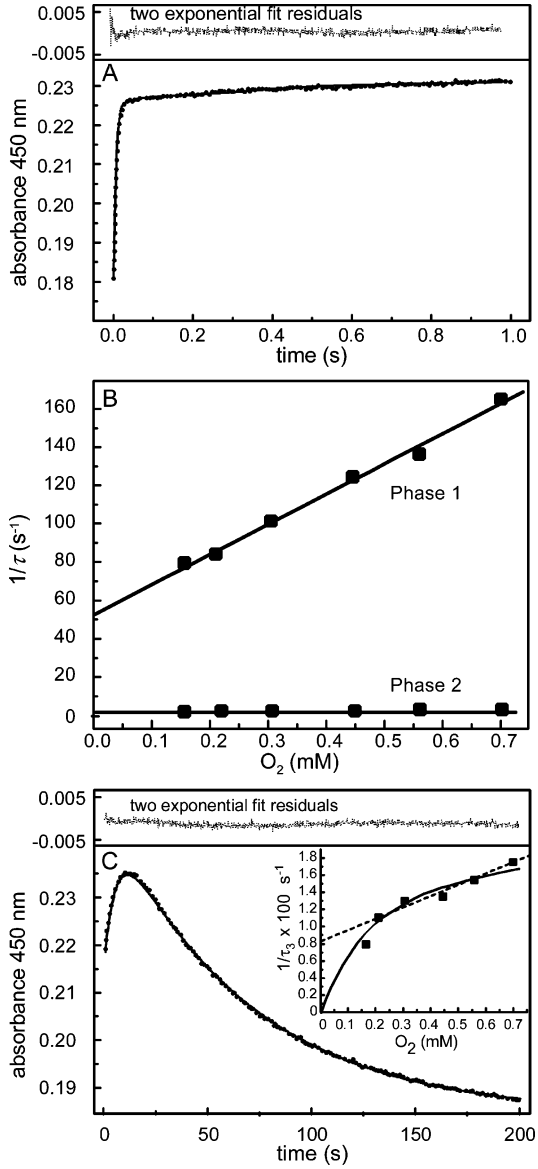

FIGURE 5: Reaction of preformed H200N−4NC upon exposure to O_2. (A) Single wavelength time course record over a 1 s time interval. The trace was best fit by two summed exponentials as shown in the panel above the time course. (B) Dependence of the observed RRTs on O_2 concentration. An expanded view shows no concentration dependence for phase 2 (view not shown). (C) Time course as in panel A recorded over a 200 s interval (the true first phase was completed prior to the first data point on this time scale). The observable part of the time course was best fit by two summed exponentials as shown. The slowest phase exhibits an O_2-concentration dependence as shown in the inset. However, it is not clear whether the dependence is linear or hyperbolic, so both possibilities are shown. Reaction conditions are as described for Figure 4. Approximately every 5th point (dots) is shown for the data sets.

as shown in Figure 5B, the second RRT does not show a dependence on O_2 concentration, which is not possible for a two-step reaction where the first step is fully reversible and not saturated, as appears to be the case here. It may be that this is actually a three- (or more) step reaction in which the second step is irreversible and causes little absorbance change. However, another possibility is suggested by the concentration dependence of a slow third phase in the reaction time course described below.

A time segment of the diode array traces of the reaction in the 10−100 s range is shown in Figure 4C. It is characterized by a large absorbance decrease in the 506 nm region coincident with an increase at 400 nm and an isosbestic point at 440 nm. A single wavelength trace, recorded at 450 nm over a 200 s time course, is shown in Figure 5C. Over this time course, fits to the second and third phases could be obtained (the first phase is essentially complete). The RRTs derived from a two exponential fit of the data when the O_2 concentration was 700 μM are $1/\tau_2 = 0.17\ s^{-1} \pm 0.02$ and $1/\tau_3 = 0.016 \pm 0.003\ s^{-1}$ as summarized and compared to the values for WT 2,3-HPCD in Table 4. The 0.17 s^{-1} phase is probably the same as the 0.22 s^{-1} phase described above, but more accurately determined due to the inclusion of more points from the relevant time domain. This phase was again

Table 4: Rate Constants or RRTs for the Reaction of the Stoichiometric, Preformed E−4NC or E−HPCA Complex with O_2

substrate	$k_{O_2\ binding}$	$1/\tau_2$ (s^{-1})	$1/\tau_3$ (s^{-1})	$k_{product\ release}$ (s^{-1})	k_{cat} (s^{-1}), 4 °C
4NC[a]					
WT 2,3-HPCD[b]	fast	1.8 ± 0.1	0.31 ± 0.03	0.07 ± 0.02	0.05
H200N	$k_{binding} = (1.5 \pm 0.2) \times 10^5\ M^{-1}s^{-1}$ $k_{release} = 52 \pm 5\ s^{-1}$	0.17 ± 0.02[d]	0.022 ± 0.003[c]	<0.0027[e,f]	0.0015
HPCA[g]					
WT 2,3-HPCD[b]	fast	38 ± 3[d]	3.2 ± 0.2[d]	nr[h]	3.2
H200N	$k_{binding} = (7.0 \pm 0.5) \times 10^5\ M^{-1}\ s^{-1}$ $k_{release} \approx 0$	5 ± 0.8[d]	0.5 ± 0.2[d]	nr[h]	0.26
H200A	$k_{binding} = (1.1 \pm 0.4) \times 10^6\ M^{-1}\ s^{-1}$ $k_{release} \approx 0$	3.3 ± 1.1[d]	0.1 ± 0.05[d]	nr[h]	0.02
H200E[i]	fast[k]	5 ± 0.8[d]	0.7 ± 0.2[d]	0.04 ± 0.01[d,j]	0.04[j]
H200F	$k_{binding} = (8.9 \pm 0.2) \times 10^5\ M^{-1}\ s^{-1}$ $k_{release} \approx 0$	~70	0.5 ± 0.2[d]	0.02 ± 0.01[d]	0.02

[a] Conditions: pH 7.5, 4°C, 20 μM 2,3-HPCD and 4NC or HPCA. The reaction was monitored at 450 nm. [b] Data for WT 2,3-HPCD from ref *12*. [c] O_2-concentration dependent. Value shown is for 700 μM O_2. [d] O_2-concentration independent. [e] Estimate. This is likely to be the overall rate-limiting step, which is 0.0015 s^{-1} from steady-state kinetic experiments. [f] The product is not the same as that from WT 2,3-HPCD. [g] Conditions: pH 7.5, 4 °C, 100 μM 2,3-HPCD and 4NC or HPCA. The reaction was monitored at 450 nm. [h] Not resolved from preceding step. [i] Data for reaction at pH 7.0. At pH 7.5, the rate-limiting reaction is much slower, and at pH 8, no individual steps are resolved in the very slow reaction. [j] pH dependent, increasing as pH decreases. [k] Although accurate values could not be obtained, a portion of these reactions could be observed in the millisecond range. Thus, they occur more slowly than in the case of WT 2,3-HPCD.

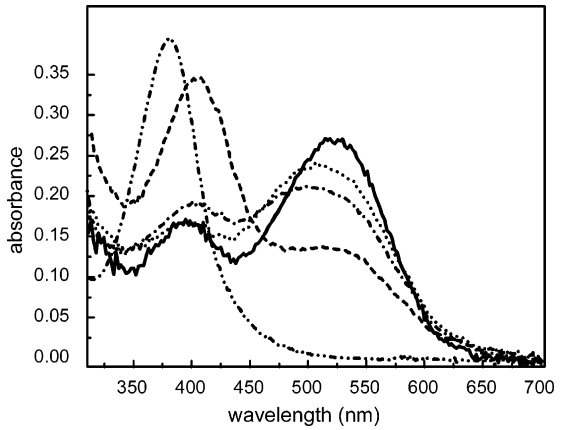

FIGURE 6: Intermediates in the reaction of preformed H200N−4NC upon exposure to O_2. Shown are the apparent spectra of the initial complex (solid line), first intermediate (dotted line), second intermediate (dash−dot line), third intermediate (dashed line), and the final product after dissociation from the enzyme (dash−dot−dot line). The analysis of the kinetic data suggests that little of the second intermediate accumulates and that it has a low extinction coefficient, so the apparent spectrum is likely to be a composite of other species. Reaction conditions are as described for Figure 4.

found to be independent of the O_2 concentration, but the slowest phase is O_2-dependent as shown in the inset to Figure 5C.

Due to the limited range over which the oxygen concentration can be varied while pseudo first order conditions are maintained, it is not possible to determine with certainty whether the O_2-concentration dependence for the slowest phase seen in Figure 5C is linear or hyperbolic. Both possibilities are illustrated in the Figure 5C inset. However, several facts suggest that the dependence is hyperbolic, and that the $1/\tau_3$ data give information about the rate constants for the second step in a linear series of reactions rather than the third. First, the changes in the optical spectra of the intermediates seen in Figure 4 and summarized in Figure 6 suggest that a different kind of conversion occurs at each step. In other words, it is unlikely that there are two forms of the final E−4NC complex binding O_2 at different rates as would be suggested by the observation of two RRTs with linear O_2-concentration dependencies. Second, the irreversible step needed to uncouple the second RRT from the O_2-concentration dependence of the first RRT would also uncouple the third RRT unless the latter actually reflects the rate constants of a slow second step in the reaction. If this is the case, then the analysis of the hyperbolic fit using eq 1 gives a $K_d = 285 \pm 50$ μM for the preceding O_2 association step, similar to the value of 340 μM determined directly from the forward and reverse rate constants for this step. The hyperbolic fit also gives a forward rate constant of 0.022 ± 0.004 s^{-1} for the slow step and a reverse rate constant of roughly zero. The irreversible nature of this step would uncouple the second largest RRT, as observed. It is somewhat counterintuitive that the exponential phase which dominates the time course for disappearance of an intermediate, in fact, gives the rate constant for its formation, but this is common in analysis of transient kinetic data.

Scheme 4: Proposed Steps and Rate Constants for the Second Half of the Single Turnover Cycle of the H200N Catalyzed Oxidation of 4NC

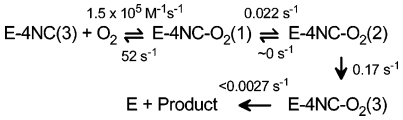

The diode array spectra in the time segment presented in Figure 4D show that there is a final step in the reaction in which the 400 nm optical maximum shifts slightly to the blue with an isosbestic point at about 425 nm. When the enzyme is incubated with excess 4NC in aerobic buffer for several turnovers, the absorbance maximum appears at 380 nm. Consequently, it is likely that the process represented by Figure 4D is product release, and the species absorbing at 400 nm is the enzyme−product complex. The process is too slow to determine an accurate relaxation time using transient techniques, but the half-life is in excess of 260 s at 4 °C, giving a rate constant of less than 0.0027 s^{-1}. This is in accord with the turnover number of 0.0015 s^{-1} at 4 °C estimated from steady-state turnover, and thus this represents the overall rate-limiting step. A summary of the proposed steps in the second half reaction is presented in Scheme 4.

Novel Product from 4NC Turnover. The diode array traces of Figure 4C,D show that the species that rapidly forms in

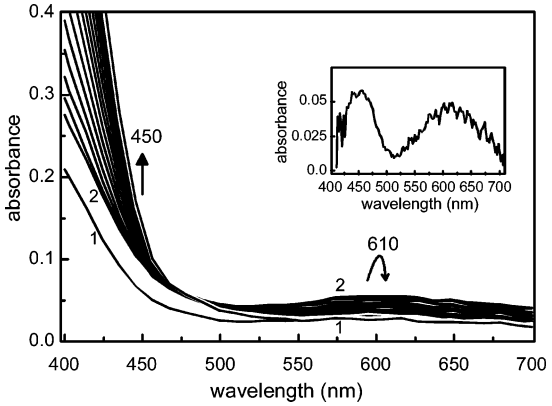

FIGURE 7: Diode array spectra of the early phases of the turnover reaction of preformed H200N−HPCA with O_2. The preformed complex and O_2 were present at 100 μM and 700 μM, respectively, after mixing. The reaction was performed in 50 mM MOPS, pH 7.5 and monitored at 4 °C. The spectrum shown in the inset is a difference spectrum in which the first spectrum recorded (at 2.5 ms) was subtracted from the predicted spectrum of the first intermediate, obtained by a global SVD analysis of the diode array data. The first two spectra recorded are numbered for ease of identification.

the 506 nm region does not decay to near zero absorbance as is observed during a single turnover of 4NC by WT 2,3-HPCD (*12*). Also, while the product from H200N absorbs in the same general region as the usual product, the λ_{max} is at 400 nm rather than 390 nm and the expected shoulder at 330 nm is not observed. When separated from the enzyme, this species absorbs at 380 nm and shows no absorbance in the 506 nm region as shown in Figure 6. This product species has been identified as the quinone of 4NC in studies that will be published elsewhere in the context of the products from several other alternative substrates for the H200X mutants.[2]

Single Turnover of Preformed H200X−HPCA Complexes upon Exposure to O_2. Although the use of 4NC as a substrate provides an excellent spectroscopic probe for steps throughout the single turnover cycle of 2,3-HPCD, its intense absorbance may mask the weaker charge transfer chromophores that arise due to the interaction of reactants and intermediates with the iron. In particular, oxygen adducts often exhibit weak chromophores that might be detectable in the absence of a substrate chromophore. The studies reported above suggest that the oxygen reaction with the H200N mutant is directly observable when 4NC is the substrate, and thus, the resulting oxygen complex might be detectable. This was pursued using the natural substrate of 2,3-HPCD, HPCA, which is colorless in the visible prior to ring cleavage. The ring cleavage product absorbs strongly at 390 nm, but the chromophore drops to near zero absorbance at wavelengths above 470 nm.

The preformed, stoichiometric complexes of H200A, H200E, H200F, or H200N with HPCA were reacted with a large excess of O_2 to give a single turnover reaction. Diode array traces of the time course of one of these reactions in the long wavelength region using H200N are shown in Figure 7. An intermediate absorbing in the 600 nm range rapidly forms and decays as the much more intense yellow chromophore of the product forms in the 400 nm region. The

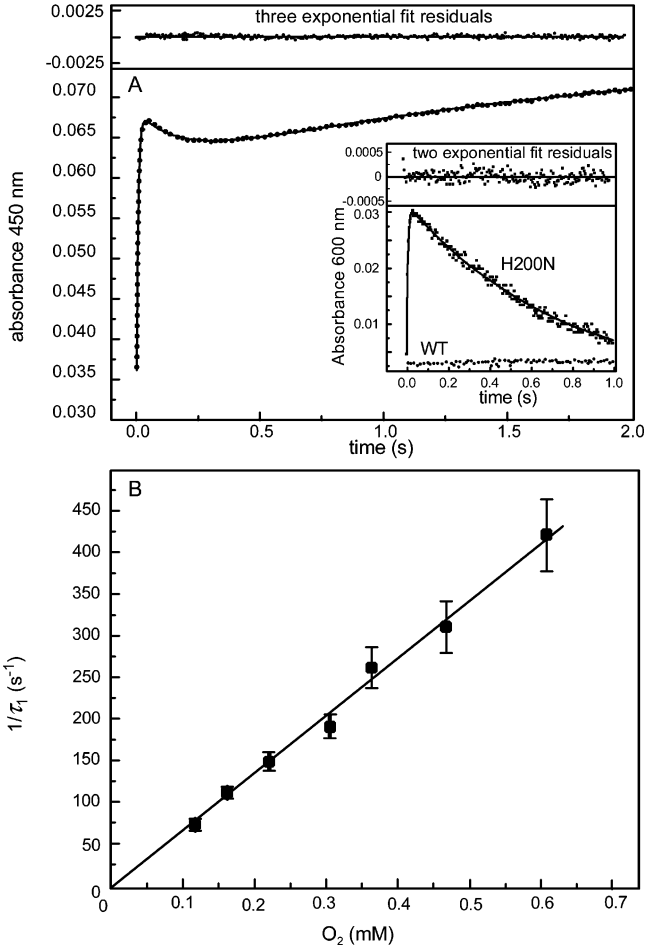

FIGURE 8: Single wavelength time course of the reaction of preformed H200N−HPCA with O_2. 50 μM H200N−HPCA complex (sites after mixing) was reacted with O_2 in 50 mM MOPS, pH 7.5, 4 °C. Panel A shows the time course recorded at 450 nm using 700 μM O_2 (after mixing). The inset shows the same time recorded at 600 nm and the time course of the reaction of preformed WT 2,3-HPCD−HPCA with O_2 for comparison. Panel B shows the O_2-concentration dependence of the first phase of the H200N−HPCA reaction. Approximately every 5th point (dots) is shown for the data set.

spectrum of the first intermediate from SVD global analysis fitting of the data is shown in the inset. This species shows absorbance maxima at 450 nm and at 610 nm.[3]

By following the reaction at 450 nm, a single time course records the formation and decay of the new intermediate as well as the product formation and release. Figure 8A shows a typical time course and a fit to three summed exponentials, the minimum required for an adequate fit. For H200N, H200F, and H200A, the first phase could be adequately fit and shows a linear dependence on O_2 concentration as illustrated in Figure 8B and summarized in Table 4. The observation of a linear plot suggests that the actual O_2 binding step is being observed for the HPCA reaction as in the case of the 4NC reaction, in this case by direct observation of the active site Fe(II)−O_2 complex. The slope of the plot gives a second order rate constant for O_2 binding of $(7.0 \pm 0.5) \times 10^5$ M^{-1} s^{-1} for the H200N mutant. The intercept near the origin suggests that the reaction is essentially irreversible.

[2] S. L. Groce and J. D. Lipscomb, in preparation.

[3] The putative oxy species also appears to exhibit an absorption band at 330 nm, although poor signal to noise in this region has thus far allowed only a qualitative evaluation.

Similar values are observed for the H200A and H200F mutants (Table 4). The fast phase was also slow enough to be detected in the time course for the reaction of H200E, but accurate RRTs could not be determined. The observation of three kinetic phases shows that there are at least three steps in the reaction. The fact that there is only one phase with a linear O_2-concentration dependence favors a mechanism like that shown in Scheme 4 in which the steps occur in sequence.

The second and third phases of the reaction are not dependent on the O_2 concentration for the reactions of any of the mutants listed in Table 4. The fact that the slowest phase of the reaction shifts from being O_2-concentration dependent in the case of the 4NC reaction to concentration independent for the HPCA reaction supports the hypothesis developed above that the slowest phase of the E−4NC reaction with O_2 actually gives information about the second step in the product forming part of the reaction cycle. The irreversible O_2 binding step in the case of HPCA causes the loss of the O_2-concentration dependence in phases that reflect the rate constants of downstream steps.

The correlation between the fastest and slowest RRTs and the rate constants for the formation and decay of the new intermediate can be explored further by following the reaction at 600 nm, where it is the only strongly absorbing species (Figure 8A, inset). Only two exponentials are required to fit the time course in this case. The faster exponential has the same RRT as the fast phase for the 450 nm data, while the slower phase correlates with the slowest 450 nm phase.

The large difference between the formation and decay rates of the intermediate suggests that it forms in nearly stoichiometric yield at high O_2 concentration. If this is the case, the extinction coefficient at 610 nm is approximately 600 M^{-1} cm^{-1}.

Rate-Limiting Step. The rate-limiting step in the catalytic cycle appears to be product release when 4NC is used as the substrate for both WT 2,3-HPCD and H200N because there is a good correlation with the k_{cat} for the multiple turnover reaction as shown in Table 4. When HPCA is the substrate, product release is likely to be the rate-limiting step for the catalytic cycles of each of the His200 mutants tested. However, a step before product release appears to be rate limiting for WT 2,3-HPCD (*12*). This suggests that His200 plays an important role in the product release process. Preliminary pH dependence studies show that both the k_{cat} value and the rate constant for the product release step of H200E increase as the pH decreases, consistent with a role for the position 200 residue as an active site acid. However, for WT 2,3-HPCD and each of the other mutants tested, the rate constant increases with increasing pH showing that another active site residue can also play this role.

DISCUSSION

The studies reported here were designed to probe the catalytic role or roles of the conserved, second-sphere, active site histidine of extradiol dioxygenases. The transient kinetics of a single turnover of variants of 2,3-HPCD in which residue His200 was mutated were studied by using the chromophoric changes that occur as the alternative substrate 4NC passes through the steps in the catalytic cycle. Also, the chromophore of the ring cleavage reaction product was used to study the last half of the reaction cycle using the natural substrate HPCA. The results show that His200 exerts only subtle effects on the substrate binding and ionization process, but has a major effect on rate constants, and, in the case of 4NC, the product obtained from the O_2 binding and reaction portion of the cycle. Significantly, the alteration in rate constants allows the detection of a new intermediate in the oxygen binding process, which appears to contain the key reactive oxygen species of the reaction cycle. These results are discussed here in the context of proposals for the extradiol dioxygenase mechanism.

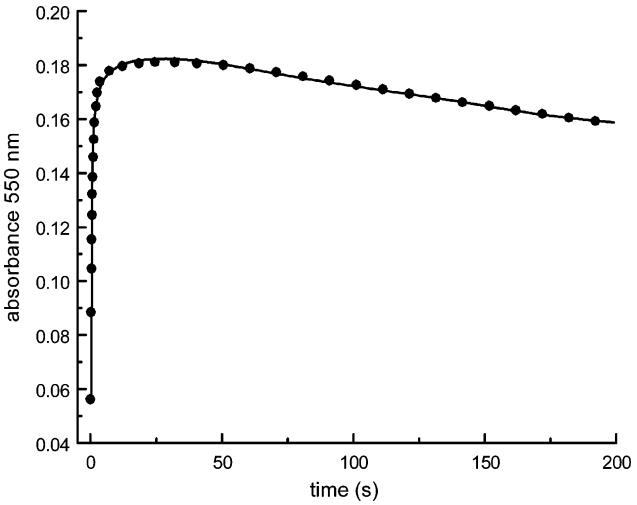

FIGURE 9: Time course for the complete single turnover reaction (dots) compared with a numerical integration simulation (solid line) based on Scheme 5 using the rate constants shown in Schemes 3 and 4 and the extinction coefficients derived from Figures 1, 6, and diode array data of the binding half-reaction. Approximately every 30th point is shown for the data set.

Scheme 5: Proposed Steps for the Complete Single Turnover Cycle of the H200N Catalyzed Oxidation of 4NC

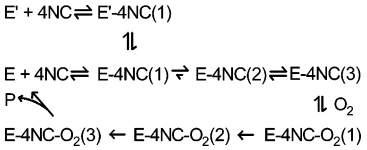

Complete Single Turnover Cycle. The kinetics of the two half-reactions using 4NC as a substrate can be studied in detail because pseudo first order conditions that allow multiple exponential fitting can be established. This is not possible for the complete single turnover cycle because supplying both substrates in excess would allow multiple turnovers to occur. However, the complete reaction can be studied by using limiting concentrations of the substrates and then employing trial and error numerical integration fitting to evaluate the rate constants. In the case of the WT enzyme, simply appending the equivalent of Scheme 4 to Scheme 2 such that the final E−4NC(3) complex reacts with O_2 to initiate the second part of the reaction allows the time course data to be fit under all conditions with the same rate constants and extinction coefficients for the intermediates. Similarly, the steps shown in Scheme 5 allow a good fit for the reaction of H200N + 4NC + O_2, an example of which is shown in Figure 9. Importantly, each of the slow steps in the half-reactions must be included to give an adequate fit. The ability to simulate the complete turnover cycle using data from the

Scheme 6: Comparison of the Catalytic Cycles for H200N Catalyzed Single Turnover of 4NC (Left) and HPCA (Right)[a]

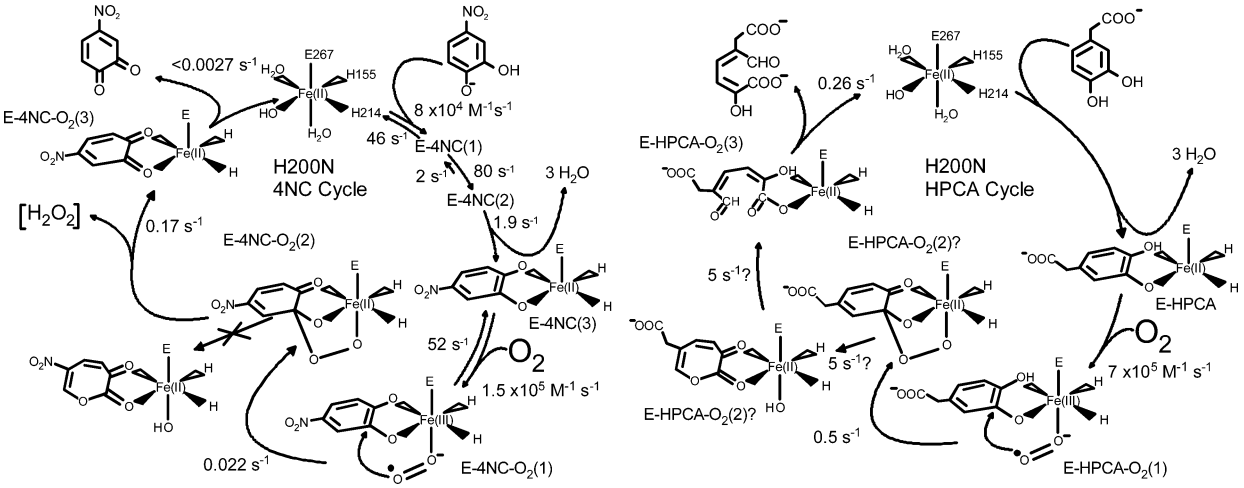

[a] The structures of the intermediates are hypothetical, but are consistent with the optical properties of the intermediate species observed. The structure best associated with E−HPCA−O_2(2) remains unclear, so two possibilities are labeled. The slow alternative 4NC binding pathway is omitted for clarity.

half-reactions shows that the intermediates recognized in the half-reactions are mechanistically relevant.

The intermediates from Scheme 5 and the differences in rate constants and products formed by the mutant enzymes used here allow a hypothesis for the mechanistic cycle to be formulated. It is illustrated in Scheme 6 for the H200N mutant turning over 4NC (left) or HPCA (right). The basis for these cycles is described in the following sections.

Role of His200 in Substrate Binding. The present results show that residues other than His can be placed at position 200 without affecting the nature of the intermediates formed during the 4NC binding process or the final stable complex that results. Specifically, residues that cannot act as an active site base are capable of replacing His200 in the substrate binding process, showing that it does not act as the catalytic base to deprotonate 4NC as it binds to the iron. Moreover, each of the mutants is capable of binding and accelerating the specific oxidative ring cleavage of HPCA, suggesting that His200 is also not critical for binding HPCA in the correct state. Thus, it appears that the primary roles of His200 lie in the second half-reaction.

This conclusion differs from that reached for the extradiol cleaving 2,3-dihydroxyphenypropionate 1,2-dioxygenase (MhpB) isolated from *E. coli* (*21*). In the studies of this enzyme, the equivalent to His200, His179, was replaced by Gln, Ala, and Tyr to yield inactive enzyme. On the basis of steady-state kinetic studies of residues thought to hydrogen bond to His179, it was concluded that this residue acts as a catalytic base to allow substrate to bind as a monoanion. While it may be that the role of this residue differs in these two enzymes, the fact that it is completely conserved in the extradiol dioxygenases suggests that this is not the case. Since substrate binding was not directly assessed in MphB, it is possible that the normal complex forms, but the reaction cannot proceed further due to structural constraints.

Role of His200 in Oxygen Binding. For WT 2,3-HPCD, transient kinetic techniques failed to reveal the O_2 binding step (*12*). It is shown here that substitution of His200 by an Asn, Phe, or Ala has the effect of slowing down the decay and/or speeding up the formation of the oxygen intermediate (see below) such that it accumulates to observable levels within the time domain of stopped-flow. In the case of the WT enzyme, O_2 binding appears to be irreversible when either HPCA or 4NC is used as the substrate because there is no O_2-concentration dependence observed in the phases of the time course for the product formation. The irreversible step could be the O_2 binding reaction itself or any following reaction before the first observable change in the optical spectrum of the bound substrate. In the case of the His200 mutants, where the second order O_2 binding step can be directly observed, it appears to be effectively irreversible when the enzyme is oxidizing HPCA. This may mean that it is also irreversible in the WT enzyme reaction. Because the oxygen binding step proceeds at a substantial rate in the absence of His200, it is likely that this residue plays a relatively minor role in this process.

The data presented here suggest that the nature of the substrate has a major effect on the rate constant for the stability of the oxygen complex once it is formed. This is in accord with our proposed mechanism for extradiol dioxygenases in which electron donation from the substrate to the iron promotes formation of a strong O_2 bond, thereby ordering the addition of substrates to the metal (*10*, *14*). When the strongly electron withdrawing nitro group is present, the ability of the iron to form a stable bond with oxygen is compromised, leading to reversible formation of the complex. Apparently, His at position 200 can compensate for the presence of a strongly electron withdrawing substituent on the substrate to allow an effectively irreversible Fe(II)−O_2 complex to form, presumably by hydrogen bonding to the bound oxygen.

Nature of the Oxygen Intermediate. Given that the X-ray crystal structure of E−HPCA(3) shows it to have only one open coordination site and that there is abundant structural and spectroscopic evidence for NO binding directly to the iron in this site in related enzymes (*7*, *28*), it is likely that the initial complex with O_2 is an end-on metal−superoxo species. The electron density transferred to the oxygen could come from the Fe(II) or from the substrate via the iron. Since the oxygen complex reported here has a weak chromophore, it is likely that the iron has taken on at least some Fe(III) character (formally Fe(III)−$O_2^{\bullet-}$), but this would probably

facilitate some degree of electron transfer from the substrate as well.

There are very few well-characterized metal−superoxo complexes for mononuclear Fe(III)-containing enzymes and model complexes. Recently, a particularly relevant series of model complexes based on the *trans*-*N*,*N*′-bis(2-pyridylmethyl)-X chelate structure, where X represents a variety of iron binding moieties such as glycine (bpmcn), have been synthesized (*29*). These molecules bind a catechol analogue and O_2 to form an intermediate that breaks down to yield extradiol products along with other species. The oxygen intermediates in these reactions exhibit optical chromophores in the range of 535 to 600 nm with extinction coefficients on the order 2000 M^{-1} cm^{-1} arising from ligand-to-metal charge transfer from the associated catecholate ligand. This is consistent with the spectrum of the intermediate described here, although the extinction coefficient of this species is not as large.

It is also possible that that both the substrate and the iron give up an electron to form an Fe(III)−peroxo or hydroperoxo intermediate. A peroxo−intermediate would also be formed if the initial metal−superoxo species immediately reacts with the nearby substrate yielding an Fe(II)−alkyl−peroxo complex, or, less likely, an Fe(III)−alkyl−peroxo species by delocalization of the electron away from the iron. Several end-on Fe(III)−peroxo complexes in model complexes and enzymes have been characterized (see, for example, ref *30*). These species have optical spectra that depend on the spin state of the iron as well as the ligand structure. For the low spin complexes, the λ_{max} values are typically near 550 nm with extinction coefficients close to 1200 M^{-1} cm^{-1}. The high spin complexes typically have λ_{max} values between 560 and 760 nm with extinction coefficients between 450 and 1200 M^{-1} cm^{-1}. The properties of the high spin complexes would be a good match for those of the intermediate observed here. Relatively few Fe(III)−alkyl−peroxo and no Fe(II)−alkyl−peroxo species have been reported. One example of the former is the product complex of soybean lipoxygenase for which the end-on Fe(III)−alkylperoxo complex has been structurally characterized (*31*). This species has an absorbance maximum at 585 nm with an extinction coefficient of 1300 M^{-1} cm^{-1} (*32*), again in accord with the oxy intermediate reported here. Similar results have been obtained for model Fe(III)−alkylperoxo complexes, which exhibit λ_{max} values ranging from 510 to 550 nm depending upon the iron ligands in the chelate complex and extinction coefficients of around 2000 M^{-1} cm^{-1} (*33*, *34*).

The spectral similarity of the catecholate−Fe(III)−superoxo, Fe(III)−peroxo, and Fe(III)−alkylperoxo moieties does not permit unambiguous assignment of the oxygen adduct reported here without additional EPR and resonance Raman studies, which are in progress. However, some insight into the nature of this intermediate can be gained from consideration of the reaction of H200N using 4NC as the substrate. In this case, the optical spectrum of the 4NC in the intermediate is similar to that of the aromatic dianion. This would be unlikely if either the Fe(III)−peroxo substrate radical species or the Fe(II)− or Fe(III)−alkylperoxo species had formed because the aromaticity of the 4NC ring would be lost. Thus, it seems most likely that the chromophoric species is the catecholate−Fe(III)−superoxo complex in which the iron is also chelated by dianionic 4NC.

Scheme 7: Proposal for the Assignment of Rate Constants for the Reactions of WT 2,3-HPCD and Mutant Enzymes in the Second Half-Reaction with HPCA as the Substrate

E-Oxy → {E- Alkyl-peroxy or E- lactone} → E-Product → E + Product

WT	38 s^{-1}	3.2 s^{-1}	>3.2 s^{-1}
H200N	0.5 s^{-1}	5 s^{-1}	0.26 s^{-1}
H200A	0.1 s^{-1}	3.3 s^{-1}	0.02 s^{-1}
H200E	0.7 s^{-1}	5 s^{-1}	0.04 s^{-1}

Role of His200 in the Reaction of the Oxygen Intermediate with Bound Substrate. After formation of the putative 4NC−Fe(III)−superoxo species in H200N, the optical chromophore from 4NC decreases in intensity with an O_2-concentration-dependent rate constant of 0.022 s^{-1} (see Results for qualifications in making this assignment). When the same reaction is followed using HPCA as the substrate, the loss of the chromophore of the oxygen-bound intermediate can be monitored directly in the 600 nm region and the rate constant is 0.54 s^{-1}. A reasonable hypothesis for loss of the chromophore is that attack of the Fe(III)−superoxide on the substrate results in an Fe(II)−alkylperoxo intermediate. LMCT interactions from either the catecholate ligand or the peroxo moiety would be expected to be much weaker to the Fe(II), and thus a nearly colorless intermediate would be anticipated. The lower rate of the 4NC reaction might be due to a decreased ability of this substrate to transfer charge to the developing Fe(III)−superoxide species making it a less powerful nucleophile.

On the basis of this interpretation, the key to detection of the oxygen-bound intermediate in the mutant enzymes is its slow reaction with substrate. For the WT enzyme, neither the 4NC nor the HPCA reaction yields a detectable intermediate. It is possible that this is due to a slow binding reaction of O_2, but this seems unlikely on the basis of the results presented here for O_2 binding to the mutants as well as precedent from a wide range of oxygenases. The more likely explanation is that the nearly colorless Fe(II)−alkylperoxo state is rapidly formed.

It is informative to consider which of the rate constants derived from the RRTs for the WT 2,3-HPCD reaction with HPCA listed in Table 4 applies to this reaction. If the relatively slow rate constant of 3.2 s^{-1} applies, then one would expect to detect oxygen adduct, which is not the case. Consequently, it is likely that the rate constant of 38 s^{-1} applies, as proposed in our previous study (*12*) (See Scheme 7). It is also possible that this initial attack on the substrate is even faster, and the 38 s^{-1} rate constant pertains to the following Criegee rearrangement reaction. In either case, this would imply a significant role for His200 in accelerating this initial attack of the bound superoxide on the substrate, since it represents a 55−380-fold increase over the rate constants observed for the mutated enzymes. One such role might be to act as an acid catalyst or to provide an optimized hydrogen bonding orientation to stabilize the developing negative charge on the bound oxygen as illustrated in Scheme 8. This would also offset the electron withdrawing effect of the nitro group in the case of the 4NC reaction accounting for the significantly higher rate constant for the WT 2,3-HPCD at this step.

Role of His200 in the Reaction of the Putative Alkylperoxo Intermediate. After the formation and decay of the oxygen intermediate, the reactions for 4NC and HPCA diverge to

Scheme 8: Potential Roles of His200 in the O_2 Insertion Reaction

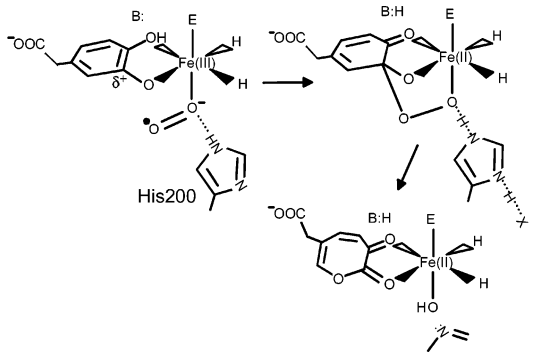

yield different types of products in the case of the H200N (and H200A and H200F) mutants, but not in the case of the WT enzyme, implying a role for residue His200 in directing product formation. We have proposed that, in the case of the WT enzyme, the alkylperoxo intermediate undergoes a Criegee type rearrangement resulting in O−O bond cleavage and oxygen insertion into the aromatic ring followed by ring opening (*10*, *14*, *35*). The rate constant for the slow step in this series of reactions for the WT enzyme, proposed here to be 3.2 s^{-1}, apparently changes very little for the mutant enzymes in the HPCA reaction (Scheme 7). It may be that this slow step is the breakdown of the lactone intermediate from the Criegee rearrangement, because this is proposed to occur by attack of the metal-bound water on the intermediate, and this could occur without participation of another active site residue. Once the lactone forms, it is likely that the reaction is committed to ring opening. Thus, the current results suggest that His200 is critical to the Criegee rearrangement chemistry only in the case of a nonoptimal substrate.

The Criegee rearrangement would be facilitated by either electron supply from the substrate side or electron withdrawal on the oxygen side. Also, stabilization of the negative charge on the metal-bound oxygen after O−O bond cleavage will facilitate the reaction. Consequently, the presence of the nitro group of 4NC in combination with the loss of a potential acid catalyst at position 200 near the oxygen might strongly inhibit the oxygen insertion chemistry. The presence of the carboxylate of HPCA or the histidine at position 200 appears to be sufficient to allow the insertion reaction to occur. In the absence of a histidine at position 200, it is likely that a proton would be transferred to the oxygen anion bound to the iron from solvent or from another active site acid catalyst, but this may not occur rapidly enough to compete with oxidation to the quinone in the case of 4NC. Moreover, evidence for another active site acid catalyst has recently been presented in the case of MhpB (*21*).

The reaction of the H200F using HPCA as the substrate exhibits a RRT of ∼70 s^{-1} for one of the steps following oxygen binding, which is comparable to that assigned for the putative Fe(III)−superoxo species with substrate in the WT 2,3-HPCD reaction. However, the formation of the oxy intermediate can be observed for this mutant, suggesting that the high rate constant applies to a later step in the cycle. If this is the case, then the 0.5 s^{-1} RRT observed for this mutant (Table 4) may describe the attack of the putative Fe(III)−superoxo species on HPCA, a value comparable to those observed for the other mutant enzyme reactions.

Role of His200 in the Product Release Reactions. Our past studies indicated that the rate-limiting step for the WT enzyme turning over HPCA occurs in one of the oxygen insertion/product formations steps (*12*). The subsequent product release step apparently occurs with a similar or greater rate constant, but it is not directly observed (*12*). In contrast, the current results show that the rate-limiting (and slow at 4 °C) step for the mutant enzymes is product release for H200E and H200F. This is likely to be the case also for H200N and H200A. Consequently, His200 may play a significant role in product dissociation, presumably by protonating the acidic product to allow rapid release. Similarly, an active site residue is suggested to serve this role by mutagenesis studies of MphB, although it is not the equivalent of His200 (*21*).

CONCLUSIONS

Structural studies have shown that His200 or its equivalent in other extradiol dioxygenases is well positioned to served as a base catalyst to deprotonate incoming substrate or as an acid catalyst for the oxygen insertion reaction. Past mechanistic proposals based on these structural studies have suggested that it may play both roles (*7*). Support for its role as a base catalyst has also come from mutagenesis studies in a related dioxygenase (*21*). In contrast, the current study shows that His200 does not serve as a base catalyst for 4NC binding in 2,3-HPCD and is unlikely to do so for HPCA binding. It does play important roles as O_2 enters the reaction especially in promoting attack of the initial oxygen adduct on the substrate and probably in product release. The nucleophilic attack of oxygen on substrate and the subsequent Criegee rearrangement reaction may involve acid catalysis as a proton is transferred to the metal-bound oxygen atom during O−O bond cleavage. These roles of His200 appear to be carried out in concert with the non-hydroxyl ring substituent of the substrate. The correct substituent can partially compensate for mutations at position 200, but alteration of both the substituent to an electron withdrawing nitro group and His200 to a non-acid−base residue leads to formation of a new product. The current findings support our previous mechanistic hypothesis in both number and chemical characteristics of the reaction cycle intermediates. They are also in accord with recent mechanistic studies based on diagnostic chemistry and density functional calculations (*29*, *36*−*39*). The latter make specific predictions about the steric organization of the putative Fe(III)−superoxo and Fe(II)−alkylperoxo intermediates with regard to the position of ring opening. The current studies should allow these intermediates to be trapped and fully evaluated for the first time by employing mutants that slow the reaction cycle at strategic steps.

REFERENCES

1. Miller, M. A., and Lipscomb, J. D. (1996) Homoprotocatechuate 2,3-dioxygenase from *Brevibacterium fuscum*—a dioxygenase with catalase activity, *J. Biol. Chem. 271*, 5524−5535.
2. Vaillancourt, F. H., Bolin, J. T., and Eltis, L. D. (2004) Ring-cleavage dioxygenases, *Pseudomonas 3*, 359−395.
3. Boldt, Y. R., Sadowsky, M. J., Ellis, L. B. M., Que, L., and Wackett, L. P. (1995) A manganese-dependent dioxygenase from *Arthrobacter globiformis* CM-2 belongs to the major extradiol dioxygenase family, *J. Bacteriol. 177*, 1225−1232.

4. Han, S., Eltis, L. D., Timmis, K. N., Muchmore, S. W., and Bolin, J. T. (1995) Crystal structure of the biphenyl-cleaving extradiol dioxygenase from a PCB-degrading pseudomonad, *Science 270*, 976−980.
5. Senda, T., Sugiyama, K., Narita, H., Yamamoto, T., Kimbara, K., Fukuda, M., Sato, M., Yano, K., and Mitsui, Y. (1996) Three-dimensional structures of free form and two substrate complexes of an extradiol ring-cleavage type dioxygenase, the BphC enzyme from *Pseudomonas sp*. Strain KKS102, *J. Mol. Biol. 255*, 735−752.
6. Sugimoto, K., Senda, T., Masai, E., Kimbara, K., Fukuda, M., and Mitsui, Y. (1999) Purification and crystallization of a catechol 2,3-dioxygenase PheB from *Bacillus stearothermophilus* BR219, *Protein Pept. Lett. 6*, 403−406.
7. Sato, N., Uragami, Y., Nishizaki, T., Takahashi, Y., Sazaki, G., Sugimoto, K., Nonaka, T., Masai, E., Fukuda, M., and Senda, T. (2002) Crystal structures of the reaction intermediate and its homologue of an extradiol-cleaving catecholic dioxygenase, *J. Mol. Biol. 321*, 621−636.
8. Vetting, M. W., Wackett, L. P., Que, L., Jr., Lipscomb, J. D., and Ohlendorf, D. H. (2004) Crystallographic comparison of manganese- and iron-dependent homoprotocatechuate 2,3-dioxygenases, *J. Bacteriol. 186*, 1945−1958.
9. Hegg, E. L., and Que, L. (1997) The 2-His-1-carboxylate facial triad: An emerging structural motif in mononuclear non-heme iron(II) enzymes, *Eur. J. Biochem. 250*, 625−629.
10. Shu, L., Chiou, Y. M., Orville, A. M., Miller, M. A., Lipscomb, J. D., and Que, L., Jr. (1995) X-ray absorption spectroscopic studies of the Fe(II) active site of catechol 2,3-dioxygenase. Implications for the extradiol cleavage mechanism, *Biochemistry 34*, 6649−6659.
11. Vaillancourt, F. H., Barbosa, C. J., Spiro, T. G., Bolin, J. T., Blades, M. W., Turner, R. F. B., and Eltis, L. D. (2002) Definitive evidence for monoanionic binding of 2,3-dihydroxybiphenyl to 2,3-dihydroxybiphenyl 1,2-dioxygenase from UV resonance Raman spectroscopy, UV/Vis absorption spectroscopy, and crystallography, *J. Am. Chem. Soc. 124*, 2485−2496.
12. Groce, S. L., Miller-Rodeberg, M. A., and Lipscomb, J. D. (2004) Single-turnover kinetics of homoprotocatechuate 2,3-dioxygenase, *Biochemistry 43*, 15141−15153.
13. Orville, A. M., and Lipscomb, J. D. (1997) Cyanide and nitric oxide binding to reduced protocatechuate 3,4-dioxygenase: Insight into the basis for order-dependent ligand binding by intradiol catecholic dioxygenases, *Biochemistry 36*, 14044−14055.
14. Arciero, D. M., and Lipscomb, J. D. (1986) Binding of ^{17}O-labeled substrate and inhibitors to protocatechuate 4,5-dioxygenase-nitrosyl complex. Evidence for direct substrate binding to the active site Fe^{2+} of extradiol dioxygenases, *J. Biol. Chem. 261*, 2170−2178.
15. Harpel, M. R., and Lipscomb, J. D. (1990) Gentisate 1,2-dioxygenase from pseudomonas. Substrate coordination to active site Fe^{2+} and mechanism of turnover, *J. Biol. Chem. 265*, 22187−22196.
16. Criegee, R. (1948) The rearrangement of decahydronaphthalene peroxide esters resulting from cationic oxygen, *Justus Liebigs Ann. Chem. 560*, 127−135.
17. Arciero, D. M., Orville, A. M., and Lipscomb, J. D. (1985) [^{17}O]-water and nitric oxide binding by protocatechuate 4,5-dioxygenase and catechol 2,3-dioxygenase. Evidence for binding of exogenous ligands to the active site Fe^{2+} of extradiol dioxygenases, *J. Biol. Chem. 260*, 14035−14044.
18. Sanvoisin, J., Langley, G. J., and Bugg, T. D. H. (1995) Mechanism of extradiol catechol dioxygenases: Evidence for a lactone intermediate in the 2,3-dihydroxyphenylpropionate 1,2-dioxygenase reaction, *J. Am. Chem. Soc. 117*, 7836−7837.
19. Spence, E. L., Langley, G. J., and Bugg, T. D. H. (1996) *Cis-trans* isomerization of a cyclopropyl radical trap catalyzed by extradiol catechol dioxygenases: Evidence for a semiquinone intermediate, *J. Am. Chem. Soc. 118*, 8336−8343.
20. Groce, S. L., and Lipscomb, J. D. (2003) Conversion of extradiol aromatic ring-cleaving homoprotocatechuate 2,3-dioxygenase into an intradiol cleaving enzyme, *J. Am. Chem. Soc. 125*, 11780−11781.
21. Mendel, S., Arndt, A., and Bugg, T. D. H. (2004) Acid-base catalysis in the extradiol catechol dioxygenase reaction mechanism: Site-directed mutagenesis of His-115 and His-179 in *Escherichia coli* 2,3-dihydroxyphenylpropionate 1,2-dioxygenase (MhpB), *Biochemistry 43*, 13390−13396.
22. Eltis, L. D., and Bolin, J. T. (1996) Evolutionary relationships among extradiol dioxygenases, *J. Bacteriol. 178*, 5930−5937.
23. Boldt, Y. R., Whiting, A. K., Wagner, M. L., Sadowsky, M. J., Que, L., Jr., and Wackett, L. P. (1997) Manganese(II) active site mutants of 3,4-dihydroxyphenylacetate 2,3-dioxygenase from *Arthrobacter globiformis* strain CM-2, *Biochemistry 36*, 2147−2153.
24. Tyson, C. A. (1975) 4-Nitrocatechol as a colorimetric probe for non-heme iron dioxygenases, *J. Biol. Chem. 250*, 1765−1770.
25. Whittaker, J. W., Orville, A. M., and Lipscomb, J. D. (1990) Protocatechuate 3,4-dioxygenase from *Brevibacterium fuscum*, *Methods Enzymol. 188*, 82−88.
26. Wang, Y. Z., and Lipscomb, J. D. (1997) Cloning, overexpression, and mutagenesis of the gene for homoprotocatechuate 2,3-dioxygenase from *Brevibacterium fuscum*, *Protein Expression Purif. 10*, 1−9.
27. Hori, K., Hashimoto, T., and Nozaki, M. (1973) Kinetic studies on the reaction mechanism of dioxygenases, *Biochem. J. 74*, 375−384.
28. Roach, P. L., Clifton, I. J., Hensgens, C. M., Shibata, N., Schofield, C. J., Hajdu, J., and Baldwin, J. E. (1997) Structure of isopenicillin N synthase complexed with substrate and the mechanism of penicillin formation, *Nature 387*, 827−830.
29. Jo, D.-H., Chiou, Y.-M., and Que, L., Jr. (2001) Models for extradiol cleaving catechol dioxygenases: Syntheses, structures, and reactivities of iron(II)-monoanionic catecholate complexes, *Inorg. Chem. 40*, 3181−3190.
30. Roelfes, G., Vrajmasu, V., Chen, K., Ho, R. Y. N., Rohde, J.-U., Zondervan, C., la Crois, R. M., Schudde, E. P., Lutz, M., Spek, A. L., Hage, R., Feringa, B. L., Münck, E., and Que, L., Jr. (2003) End-on and side-on peroxo derivatives of non-heme iron complexes with pentadentate ligands: Models for putative intermediates in biological iron/dioxygen chemistry, *Inorg. Chem. 42*, 2639−2653.
31. Skrzypczak-J. E., Bross, R. A., Carroll, R. T., Dunham, W. R., and Funk, M. O., Jr. (2001) Three-dimensional structure of a purple lipoxygenase, *J. Am. Chem. Soc. 123*, 10814−10820.
32. Solomon, E. I., Brunold, T. C., Davis, M. I., Kemsley, J. N., Lee, S. K., Lehnert, N., Neese, F., Skulan, A. J., Yang, Y. S., and Zhou, J. (2000) Geometric and electronic structure/function correlations in non-heme iron enzymes, *Chem. Rev. 100*, 235−349.
33. Kim, J., Zang, Y., Costas, M., Harrison, R. G., Wilkinson, E. C., and Que, L., Jr. (2001) A nonheme iron(II) complex that models the redox cycle of lipoxygenase, *J. Biol. Inorg. Chem. 6*, 275−284.
34. Costas, M., Mehn, M. P., Jensen, M. P., and Que, L., Jr. (2004) Dioxygen activation at mononuclear nonheme iron active sites: Enzymes, models, and intermediates, *Chem. Rev. 104*, 939−986.
35. Wolgel, S. A., Dege, J. E., Perkins-Olson, P. E., Jaurez-Garcia, C. H., Crawford, R. L., Münck, E., and Lipscomb, J. D. (1993) Purification and characterization of protocatechuate 2,3-dioxygenase from *Bacillus macerans*: A new extradiol catecholic dioxygenase, *J. Bacteriol. 175*, 4414−4426.
36. Deeth, R., J., and Bugg, T., D. H. (2003) A density functional investigation of the extradiol cleavage mechanism in non-heme iron catechol dioxygenases, *J. Biol. Inorg. Chem. 8*, 409−418.
37. Bugg, T. D. H. (2003) Dioxygenase enzymes: Catalytic mechanisms and chemical models, *Tetrahedron 59*, 7075−7101.
38. Lin, G., Reid, G., and Bugg, T. D. H. (2001) Extradiol oxidative cleavage of catechols by ferrous and ferric complexes of 1,4,7-triazacyclononane: Insight into the mechanism of the extradiol catechol dioxygenases, *J. Am. Chem. Soc. 123*, 5030−5039.
39. Bugg, T. D. H., and Lin, G. (2001) Solving the riddle of the intradiol and extradiol catechol dioxygenases: How do enzymes control hydroperoxide rearrangements?, *Chem. Commun.* 941−952.

BI050180V